IEEE Access
Multidisciplinary | Rapid Review | Open Access Journal

Received 27 February 2023, accepted 3 April 2023, date of publication 6 April 2023, date of current version 12 April 2023.

Digital Object Identifier 10.1109/ACCESS.2023.3265076

APPLIED RESEARCH

Multi-Objective Optimization of 1T2R Parallel Mechanisms Without Fixed Orientation Center and Axis Under the Influence of Parameter Perturbation

YANG QI, YU WANG, AND HONG WANG
School of Mechanical Engineering, Tianjin University of Technology and Education, Tianjin 300222, China

Corresponding author: Yang Qi (qiyang@tju.edu.cn)

This work was supported in part by the National Natural Science Foundation of China under Grant 51905378, in part by the Natural Science Foundation of Tianjin under Grant 20JCQNJC00360, in part by the Tianjin Enterprise Science and Technology Commissioner Project under Grant 20YDTPJC00450, in part by the Scientific Research Foundation of Tianjin University of Technology and Education under Grant KYQD1901, and in part by the Tianjin Education Commission Scientific Research Program under Grant 2020KJ105.

ABSTRACT To track moving targets and signals in space, multiple characteristics as large orientational workspace and excellent kinematic performance are required for the satellite antenna driving mechanism. Due to variable orientational center and axes, the 3-RSR mechanism is capable of 1T2R with continuous workspace and becomes a promising solution for the satellite antenna driving mechanism. Influenced by the topological structure characteristics as none fixed orientation center and axes, the performances of 3-RSR mechanism are significantly impacted by the parameter perturbation. According to the differential mapping between finite screw and instantaneous screw, the structure, kinematics, performance, and optimization are unified under the FIS theory. To be applied for the satellite antenna driving mechanism, this paper carries out the multi-objective optimization of 3-RSR mechanism under the influence of parameter perturbation based on the FIS theory. Firstly, the orientational workspace is obtained by finite screw and the instantaneous motion description of the mechanism is derived through calculation principle of FIS theory. Secondly, the orientational workspace and kinematics indices of the mechanism are proposed towards the actual requirements of the satellite antenna driving, and the relationship with the parameters is established. The discrete operation becomes extremely complex owing to parameter perturbation, and the RSMs (response surface model) of indices without considering and considering parameter perturbation are modeled. The multi-objectives optimization of 3-RSR mechanism influenced by parameter perturbation is carried out and its Pareto frontier is obtained. Finally, a point preferred strategy is proposed and the optimum value of the parameter from Pareto frontier is selected.

INDEX TERMS Parallel mechanism, multi-objective optimization, response surface model, Pareto frontier.

I. INTRODUCTION

The antenna is a necessary component to track moving targets and signals. It attaches rigidly to the output end of a mechanism and is driven to realize two rotations with large angles [1]. Nowadays, the mechanisms applied in driving satellite antenna are mainly series mechanisms. According to the number of rotating shafts, satellite antenna driving mechanisms can be divided into one axis, two axis, three axis and four axis mechanisms. Two axis mechanisms are widely used, among which the representative ones include pitching azimuth type, X-Y type and polar axis type [2]. These three kinds of mechanisms have certain singular pose, and it is difficult to adjust the pose and orientation under the accompanying motion when the fixed platform moves [3], [4]. Therefore, to solve the positioning difficulties caused by the shaking of the fixed platform one or two axes are usually added on this basis to become three-axis or four-axis

The associate editor coordinating the review of this manuscript and approving it for publication was Chun-Hao Chen.

mechanisms [5]. Note that the weight of antenna is increasing because of the demands for higher signal gain and narrower beam width [6]. The series mechanisms might not reach satisfactory accuracy performance. Therefore, it is necessary to design a satellite antenna driving mechanism based on parallel mechanisms to improve accuracy of satellite antenna driving mechanisms.

The continuous motion of the satellite antenna driving mechanism is described as one translation and two rotations (1T2R). As a representative 1T2R mechanism, the 3-RSR mechanism, without fixed orientation center and axis, with the advantages of large orientational workspace and excellent kinematics performance, is the preferred scheme to apply parallel mechanism to satellite antenna driving mechanism [7]. Wu [8] has demonstrated the advantages of using 3-RSR mechanism as driving mechanism of satellite antenna. Yulei [9] analyzed the dynamics of the 3-RSR mechanism, which is used for antenna driving under the influence of external forces, and proposed the optimization of the topological structure of the satellite antenna driving mechanism based on the 3-RSR mechanism in another paper [10]. Zhang et al. [7] studied the singularity of 3-RSR mechanism. Di Gregorio [11] made a comprehensive kinematic analysis of the 3-RSR mechanism.

Based on the previous research, 3-RSR mechanism without singularity within workspace is capable of driving satellite antenna. For the optimization of parallel tracking mechanism at the request of tracking moving targets, large and high-quality orientational workspace is the primary concern [12]. Gosselin and Angeles [13] took the area of the workspace as the performance indices and carried out scale synthesis of the 3-RSR mechanism. Moreover, kinematic performances of the parallel tracking mechanism need to be considered since the antenna is required to achieve high speed and high precision tracking [12]. The virtual power transmissibility is well recognized on account of clear physical meaning and unified dimension. Tsai [14] and Staicu [15] applied the virtual work principle to obtain the dynamic model of the 6-DOF Stewart motion platform and optimized the orientation transmission capacity of the mechanism.

Considering that both workspace and kinematics performances play a key role in the design of the mechanism, the optimization of the mechanism is a multi-objective optimization problem. The existing multi-objective optimization methods are mostly decision-making before optimization. The first way is to transform two objectives into one objective by using their internal relationship. Stock [16] and Huang [17] obtained the variation law of a single parameter with the objective function through monotonicity analysis, and finally selected the optimal value of the parameter by the constraints. The second way is to choose one or two objectives as optimization objectives and let the other objectives be constraint conditions. Based on parallel mechanism with high speed and high acceleration, Minxiu et al. [18] proposed multiple performance indices about kinematic and dynamic, and established a standard multi-objective optimization model as the objective function and constraint conditions. Although these methods can reduce the difficulty of optimization and easily obtain the optimum value of optimization objectives, the solution is not a win–win result since the indices act independently without cooperating with each other [19]. The optimization objectives of parallel mechanism are equally important [20], different indices should be equally regarded without preconception. And the relationship between internal competition and cooperation needs to be considered. Multi-objective optimization should obtain a set of multi-objective equilibrium solutions, known as the non-dominated solution set or Pareto frontier. All the solutions on Pareto frontier are deemed to be equally good [21]. Compared with the single-objective optimization method, Pareto frontier method considers multiple objectives equally, instead of abandoning some goals for the superiority ones.

In view of above issues, this paper carries out multi-objective optimization of 3-RSR mechanism considering parameter perturbation. The introduction of this paper reviews the research status of 3-RSR mechanism, satellite antenna driving mechanism, and the method of multi-objective optimization. Remainder of this paper is organized as follows: in second section, a method for multi-objective optimization of 3-RSR mechanisms under the influence of parameter perturbation is proposed. In the third section, the kinematics analysis is completed, and the two key performances of 3-RSR mechanism, orientational workspace and the virtual power transmissibility are analyzed. In the fourth section, the RSM of indices is built through design of experiment, and the analytical model of performance indices is obtained after accuracy verification. In the fifth section, considering the influence of parameter perturbation on the performance, the RSM of indices under considering parameter perturbation is established to reduce the difficulty of discrete operation. The Pareto frontier is obtained with PSO. Based on the point preferred strategy, the value of parameter of the 3-RSR mechanism is selected from Pareto frontier. The sixth section is conclusion of the paper.

II. MULTI-OBJECTIVE OPTIMIZATION PROCESS

Engineering application is the first guiding principle of mechanism optimization, and the results of mechanism optimization ultimately serve engineering application. Based on engineering requirements, the optimization process is divided into three steps, as follows (Fig.1).

Step 1: RSM models of performance indices without considering parameter perturbation

Based on the engineering application requirements, the continuous motion required by the mechanism can be described by finite screw, and multiple key performances can be determined. According to the topology of the mechanism, the normalized design parameters can be extracted. After analyzing performance with FIS theory, the RSM of indices without considering parameter perturbation can be established by design of experiment.

Step 2: Establishment of statistical objectives and probabilistic constraints

Based on RSM established in step 1, N sets of design variable are randomly generated by regarding the assigned values as mean value and the machining tolerance as the standard variance. A probabilistic constraint concerning parameter perturbation is built and RSM of indices considering parameter perturbation can be established.

Step 3: Implementation of multi-objective optimization and optimal result selection

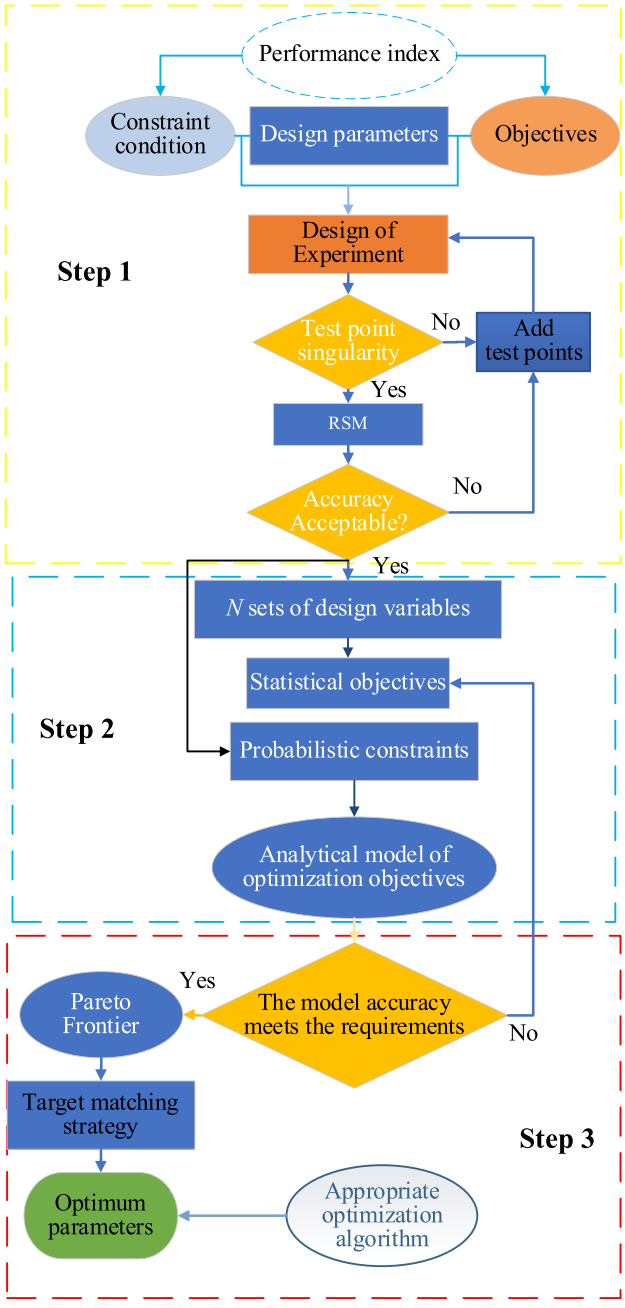

FIGURE 1. Multi-objective optimization process.

The Pareto frontier of parameters under parameter perturbation can be obtained by applying appropriate optimization algorithm. Finally, considering engineering application, optimal parameter of mechanism is obtained by appropriate point preferred strategy.

To meet the requirements of engineering applications for the stiffness, mass, workspace, etc. of mechanisms, the performance indices of mechanisms are usually diversified and complex. Consequently, the optimization of mechanisms is a multi-parameter and multi-objective nonlinear problem. Pareto frontier method considers the competition, conflict and coupling of multiple objectives, which is an advantageous solution for multi-objective optimization of parallel mechanisms.

The errors caused by processing and assembly during the manufacturing process of prototype can lead to the perturbation between the real value of parameters and the theoretical value obtained from optimization, which is called parameter perturbation. The existence of parameter perturbation can make the real performance of the physical prototype of the parallel mechanism deviate from the theoretical results of its optimization. To reduce the influence of parameter perturbation on the performance, the influence of parameter perturbation must be considered in the optimization.

The addition of parameter perturbation will greatly increase the discrete operation of optimization. RSM is a method to establish a mathematics model between optimization objectives and parameters based on the input and output relationship of the system using Design of Experience (DoE), to reduce the difficulty of discrete operation. The RSM of indices without considering parameter perturbation is the basis of the establishment of RSM of considering parameter perturbation. After the parameter perturbation is taken as the constraint added in, the RSM of mean vale of indices considering parameter perturbation is obtained. The accuracy of the first to fourth order RSMs is evaluated, and the analytical model with the highest degree is selected respectively.

III. KEY PERFORMANCE ANALYSIS

As to the satellite antenna driving mechanism, there are two key performances are most worthy of attention. To ensure the stability of signal transmission, the satellite antenna needs to orientate in a large range to find the best transmission angle. The satellite antenna drive mechanism is required to have excellent orientation capability. At the same time, the satellite antenna driving mechanism is required to have excellent kinematics performance to achieve rapid target acquisition.

A. INVERSE SOLUTION OF MECHANISM POSITION

For 3-RSR mechanism (Fig.2), the finite motion of its moving platform can be obtained in (1) by calculating the intersection of finite motions of series limbs that constitute the mechanism

with the static platform and the moving platform.

$$\boldsymbol{S}_f\,|_{3-RSR} = 2\tan\frac{\theta_a}{2}\begin{pmatrix}\boldsymbol{s}_a\\ \boldsymbol{r}_a\times\boldsymbol{s}_a\end{pmatrix}\Delta 2\tan\frac{\theta_b}{2}\begin{pmatrix}\boldsymbol{s}_b\\ \boldsymbol{r}_b\times\boldsymbol{s}_b\end{pmatrix}\Delta t_c\begin{pmatrix}\boldsymbol{0}\\ \boldsymbol{s}_c\end{pmatrix} \tag{1}$$

As shown in Fig.2, fixed coordinate system $O-xyz$ and follow-up coordinate system $P-x'y'z'$ are established at point O and P which are the center point of static and moving platforms respectively. In the fixed coordinate system, the z axis is perpendicular to the plane of the static platform, the x axis coincides with $\boldsymbol{OB}_1$, and the y axis direction is determined by the right-hand rule. At the initial pose, the axis projection of the follow-up coordinate system $P-x'y'z'$ coincides with that of the fixed coordinate system $O-xyz$. The rotating pair centers of the moving and static platforms connected with the branch i are A_i and B_i respectively. The spherical pair center of the branch i is C_i. The midpoint of the line segment OP is D. Define $\boldsymbol{p}$ for vector $\boldsymbol{OP}$. Define $\boldsymbol{d}$ for vector $\boldsymbol{PD}$. Define $\boldsymbol{a}_i$ for vector $\boldsymbol{PA}_i$. Define $\boldsymbol{b}_i$ for vector $\boldsymbol{OB}_i$. Define $\boldsymbol{c}_i$ for vector $\boldsymbol{OC}_i$. Define $\boldsymbol{m}_i$ for vector $\boldsymbol{PC}_i$. Define $\boldsymbol{h}_i$ for vector $\boldsymbol{AC}_i$. The angle between the unit normal vector $\boldsymbol{w}$ of the moving platform and the z axis is defined as the inclination angle θ, and the angle between the projection of the normal vector $\boldsymbol{w}$ in the plane xOy and the axis x is defined as the azimuth angle ϕ. Set the included angle $\kappa = \theta/2$ between z axis and $\boldsymbol{OP}$, then the coordinate of the center P of the moving platform is

$$\boldsymbol{p} = p[\mathrm{skc}\ \phi\ \mathrm{sks}\ \phi\ \mathrm{ck}]^T \tag{2}$$

where, s and c represent sin and cos respectively.

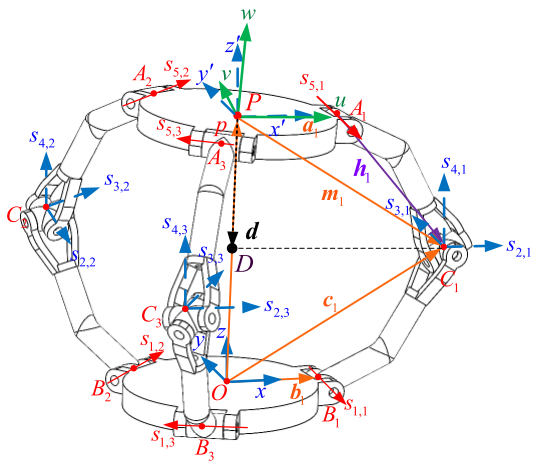

FIGURE 2. 3-RSR mechanism coordinate system.

During the movement of the mechanism, the rotation matrix $\boldsymbol{R}$ of the moving coordinate system $P-x'y'z'$ relative to the fixed coordinate system $O-xyz$ can be expressed as

$$\boldsymbol{R} = \begin{bmatrix} \mathrm{c}^2\phi\mathrm{c}\theta+\mathrm{s}^2\phi & \mathrm{s}\phi\mathrm{c}\phi\mathrm{c}\theta-\mathrm{s}\phi\mathrm{c}\phi & \mathrm{c}\phi\mathrm{s}\theta \\ \mathrm{s}\phi\mathrm{c}\phi\mathrm{c}\theta-\mathrm{s}\phi\mathrm{c}\phi & \mathrm{s}^2\phi\mathrm{c}\theta+\mathrm{c}^2\phi & \mathrm{s}\phi\mathrm{s}\theta \\ -\mathrm{c}\phi\mathrm{s}\theta & -\mathrm{s}\phi\mathrm{s}\theta & \mathrm{c}\theta \end{bmatrix} \tag{3}$$

Due to the symmetrical of the mechanism, the connecting line between D and C_i is perpendicular to the line segment OP, according to the parallel vector:

$$\boldsymbol{d}\cdot(\boldsymbol{c}_i-\boldsymbol{d}) = 0, \quad i = 1,2,3 \tag{4}$$

The inverse solution expression of the driving angle β_i can be obtained

$$\beta_1 = 2\arctan\frac{-4l\cos\kappa+\sqrt{16l^2\cos^2\kappa-4mn}}{2m} \tag{5}$$

$$\beta_2 = 2\arctan\frac{-4l\cos\kappa+\sqrt{16l^2\cos^2\kappa-4gh}}{2g} \tag{6}$$

$$\beta_3 = 2\arctan\frac{-4l\cos\kappa+\sqrt{16l^2\cos^2\kappa-4qr}}{2q} \tag{7}$$

where, β_i is the driving angle of branch i, l is the length of $\boldsymbol{h}_i$.

$$\begin{aligned} m &= (-p+2b\cos\phi\sin\kappa-2l\cos\phi\sin\kappa)\\ n &= (-p+2b\cos\phi\sin\kappa+2l\cos\phi\sin\kappa)\\ g &= -p-b\cos\phi\sin\kappa+\sqrt{3}\,b\sin\kappa\sin\phi\\ &\quad +l\cos\phi\sin\kappa-\sqrt{3}\,l\sin\kappa\sin\phi\\ h &= -p-b\cos\phi\sin\kappa+\sqrt{3}\,b\sin\kappa\sin\phi\\ &\quad -l\cos\phi\sin\kappa+\sqrt{3}\,l\sin\kappa\sin\phi\\ q &= -p-b\cos\phi\sin\kappa-\sqrt{3}\,b\sin\kappa\sin\phi\\ &\quad +l\cos\phi\sin\kappa+\sqrt{3}\,l\sin\kappa\sin\phi\\ r &= -p-b\cos\phi\sin\kappa-\sqrt{3}\,b\sin\kappa\sin\phi\\ &\quad -l\cos\phi\sin\kappa-\sqrt{3}\,l\sin\kappa\sin\phi \end{aligned}$$

B. ORIENTATIONAL WORKSPACE ANALYSIS

Orientational workspace refers to the maximum orientational workspace that the moving platform can achieve in three rotation directions after the pose of the center point of the moving platform is determined. As shown in (8), g_i describes the orientation in Gibson form. s_i is a unit vector that expresses the orientation direction from the initial orientation to the current orientation. θ_i is the orientational angle which is measured from the initial orientation.

$$g_x = 2\tan\frac{\theta_x}{2}\boldsymbol{s}_x,\ g_y = 2\tan\frac{\theta_y}{2}\boldsymbol{s}_y,\ g_{xy} = 2\tan\frac{\theta_{xy}}{2}\boldsymbol{s}_{xy} \tag{8}$$

$$\theta_{xy} = 2\arctan\left(\frac{\left|\tan\frac{\theta_x}{2}\boldsymbol{s}_x+\tan\frac{\theta_y}{2}+\tan\frac{\theta_x}{2}\tan\frac{\theta_y}{2}\boldsymbol{s}_y\times\boldsymbol{s}_x\right|}{1-\tan\frac{\theta_x}{2}\tan\frac{\theta_y}{2}\boldsymbol{s}_y^{\mathrm{T}}\boldsymbol{s}_x}\right)$$

$$\boldsymbol{s}_{xy} = \frac{\tan\frac{\theta_x}{2}\boldsymbol{s}_x+\tan\frac{\theta_y}{2}+\tan\frac{\theta_x}{2}\tan\frac{\theta_y}{2}\boldsymbol{s}_y\times\boldsymbol{s}_x}{\left|\tan\frac{\theta_x}{2}\boldsymbol{s}_x+\tan\frac{\theta_y}{2}+\tan\frac{\theta_x}{2}\tan\frac{\theta_y}{2}\boldsymbol{s}_y\times\boldsymbol{s}_x\right|}$$

$$\{\boldsymbol{g}_{\mathrm{M}}\}\subseteq\{\boldsymbol{g}_{xy}\},$$

$$\{\boldsymbol{g}_{xy}\} = \left\{2\tan\frac{\theta_{xy}}{2}\boldsymbol{s}_{xy}\,\middle|\,\theta_{xy}\in[0,2\pi],\boldsymbol{s}\in\mathbb{R}^{3\times1},|\boldsymbol{s}|=1\right\} \tag{9}$$

Therefore, $\{\boldsymbol{g}_{\mathrm{M}}\}$ is a sub-three-dimensional orientational workspace. Based on MATLAB, the maximum angle search

method is used to obtain the orientational workspace of the mechanism when constraint $t_0(\theta, \phi)$ is satisfied. $t_0(\theta, \phi)$ should include

a) Maximum rotation angle constraint: $\begin{cases} \theta_S < \theta_{S\max} \\ \theta_R < \theta_{R\max} \end{cases}$,

where $\theta_{S\max}$ and $\theta_{R\max}$ are respectively the maximum allowable rotation angle of the ball suit and the rotating pair.

b) Connecting rod interference constraint: $D > D_0$, where D_0 is the minimum safe distance.

In a plane which p is given, the reachable workspace of the maximum inclination angle $\theta_{\max} \geq 45°$ is regarded as the orientational workspace. With the help of MATLAB software, the maximum orientation angle under different values of p and three-dimensional diagrams of the orientational workspace are obtained, as shown in Fig.3 and Fig.4 respectively.

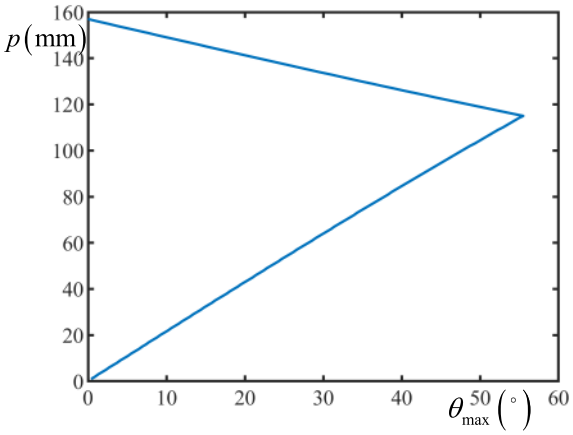

FIGURE 3. Maximum orientation angle under different values of P.

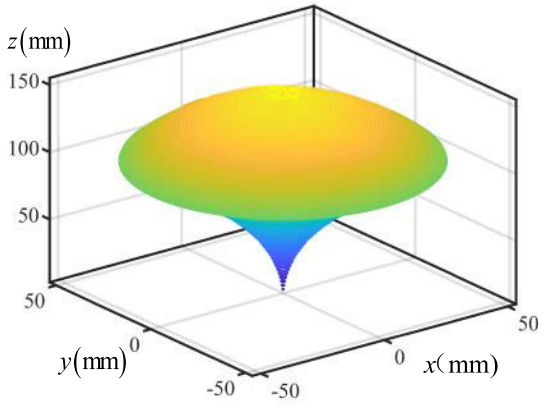

FIGURE 4. Orientational workspace of 3-RSR mechanism.

C. VELOCITY JACOBIAN MATRIX

Based on FIS theory, instant screw is the derivative of finite screw. The instant screw of the center point P of the moving platform is

$$\$_{\mathrm{t}} = \dot{\boldsymbol{S}}_{fi}|_{3-RSR} = \sum_{j=1}^{5} \rho_{i,j} \hat{\$}_{\mathrm{t},i,j} \tag{10}$$

where, $\dot{\boldsymbol{S}}_{fi}|_{3-RSR}$ is the description of continuous motion of 3-RSR mechanism based on finite screw, $\$^{\wedge}_{t,i,j}$ and $\rho_{i,j}$ respectively represent the unit velocity screw and intensity of single degree of freedom motion amplitude j in the branch i.

For branch i,

$$\hat{\$}_{t,i,1} = \begin{bmatrix} (-\boldsymbol{p}_i + \boldsymbol{b}_i) \times \boldsymbol{s}_{i,1} \\ \boldsymbol{s}_{i,1} \end{bmatrix}, \quad \hat{\$}_{t,i,2} = \begin{bmatrix} \boldsymbol{m}_i \times \boldsymbol{e}_1 \\ \boldsymbol{e}_1 \end{bmatrix},$$
$$\hat{\$}_{t,i,3} = \begin{bmatrix} \boldsymbol{m}_i \times \boldsymbol{e}_2 \\ \boldsymbol{e}_2 \end{bmatrix}, \quad \hat{\$}_{t,i,4} = \begin{bmatrix} \boldsymbol{m}_i \times \boldsymbol{e}_3 \\ \boldsymbol{e}_3 \end{bmatrix},$$
$$\hat{\$}_{t,i,5} = \begin{bmatrix} \boldsymbol{a}_i \times \boldsymbol{s}_{i,5} \\ \boldsymbol{s}_{i,5} \end{bmatrix}$$

where, $\underset{i,j}{\$}$ is the axis unit vector of the rotating pair j in the branch i, and

$$\boldsymbol{s}_{i,1} = (\mathrm{c}\vartheta_i,\ \mathrm{s}\vartheta_i, 0)\,, \boldsymbol{s}_{i,5} = (\mathrm{c}\vartheta_i, \mathrm{s}\vartheta_i, 0)\,,$$
$$\vartheta_i = -\frac{\pi}{2} + (i-1)\frac{2\pi}{3}, \quad \boldsymbol{e}_1 = \begin{bmatrix} 1 & 0 & 0 \end{bmatrix}^{\mathrm{T}},$$
$$\boldsymbol{e}_2 = \begin{bmatrix} 0 & 1 & 0 \end{bmatrix}^{\mathrm{T}}, \quad \boldsymbol{e}_3 = \begin{bmatrix} 0 & 0 & 1 \end{bmatrix}^{\mathrm{T}}$$

For the branch i, the drive screw $\hat{\$}^{\mathrm{T}}_{\mathrm{wa},i}$ and the constraint screw $\hat{\$}^{\mathrm{T}}_{\mathrm{wc},i}$ are respectively used to do the generalized inner product of the two ends of (11), which can be obtained

$$\hat{\$}^{\mathrm{T}}_{\mathrm{wa},i} \$_t = \rho_{1,1} \hat{\$}^{\mathrm{T}}_{\mathrm{wa},i} \hat{\$}_{t,1,1} \tag{11}$$
$$\hat{\$}^{\mathrm{T}}_{\mathrm{wc},i} \$_t = 0 \tag{12}$$

where,

$$\hat{\$}^{\mathrm{T}}_{\mathrm{wa},i} = \begin{bmatrix} \boldsymbol{m}_i \times \boldsymbol{s}_i \\ \boldsymbol{s}_i \end{bmatrix}, \boldsymbol{s}_i = \boldsymbol{h}_i,$$
$$\hat{\$}^{\mathrm{T}}_{\mathrm{wc},i} = \begin{bmatrix} \boldsymbol{m}_i \times \boldsymbol{s}_{c,i} \\ \boldsymbol{s}_{c,i} \end{bmatrix}, \boldsymbol{s}_{c,i} = \frac{(\boldsymbol{s}_{i,1} \times \boldsymbol{s}_{i,2}) \times (\boldsymbol{s}_{i,3} \times \boldsymbol{s}_{i,5})}{|(\boldsymbol{s}_{i,1} \times \boldsymbol{s}_{i,2}) \times (\boldsymbol{s}_{i,3} \times \boldsymbol{s}_{i,5})|}.$$

From (11) and (12), the motion mapping model of 3-RSR mechanism can be expressed as

$$\boldsymbol{J}_x \hat{\$}_t = \boldsymbol{J}_p \boldsymbol{\rho} \tag{13}$$

where,

$$\boldsymbol{J}_x = \begin{bmatrix} \boldsymbol{J}_{xa} \\ \boldsymbol{J}_{xc} \end{bmatrix}, \quad \boldsymbol{J}_p = \begin{bmatrix} \boldsymbol{J}_{pa} \\ \boldsymbol{0}_{3\times 6} \end{bmatrix}, \quad \boldsymbol{\rho} = \begin{bmatrix} \boldsymbol{\rho}_a \\ \boldsymbol{0}_{3\times 1} \end{bmatrix}$$
$$\boldsymbol{J}_{xa} = \begin{bmatrix} \hat{\$}^{\mathrm{T}}_{\mathrm{wa},1} \\ \hat{\$}^{\mathrm{T}}_{\mathrm{wa},2} \\ \hat{\$}^{\mathrm{T}}_{\mathrm{wa},3} \end{bmatrix}, \quad \boldsymbol{J}_{xc} = \begin{bmatrix} \hat{\$}^{\mathrm{T}}_{\mathrm{wc},1} \\ \hat{\$}^{\mathrm{T}}_{\mathrm{wc},2} \\ \hat{\$}^{\mathrm{T}}_{\mathrm{wc},3} \end{bmatrix},$$
$$\boldsymbol{J}_{pa} = \begin{bmatrix} \hat{\$}^{\mathrm{T}}_{\mathrm{wa},1} \hat{\$}_{t,1,1} & 0 & 0 & 0 & 0 & 0 \\ 0 & \hat{\$}^{\mathrm{T}}_{\mathrm{wa},2} \hat{\$}_{t,2,1} & 0 & 0 & 0 & 0 \\ 0 & 0 & \hat{\$}^{\mathrm{T}}_{\mathrm{wa},3} \hat{\$}_{t,3,1} & 0 & 0 & 0 \end{bmatrix},$$
$$\boldsymbol{\rho}_a = \begin{bmatrix} \dot{\theta}_1 \\ \dot{\theta}_2 \\ \dot{\theta}_3 \end{bmatrix} = \begin{bmatrix} \rho_{1,1} \\ \rho_{2,1} \\ \rho_{3,1} \end{bmatrix}.$$

The motion mapping model of the mechanism can be further expressed as

$$\hat{\boldsymbol{\$}}_{\mathrm{t}} = \boldsymbol{J}_{\mathrm{x}}^{-1}\boldsymbol{J}_{\mathrm{p}}\boldsymbol{\rho} \tag{14}$$

where,

$$\hat{\boldsymbol{\$}}_t = \begin{bmatrix}\dot{\boldsymbol{p}} & \boldsymbol{\omega}\end{bmatrix}^{\mathrm{T}}, \dot{\boldsymbol{p}} = \begin{bmatrix} \dot{p}\mathrm{s}\kappa\mathrm{c}\phi + p\dot{\kappa}\mathrm{c}\kappa\mathrm{c}\phi - p\dot{\phi}\mathrm{s}\kappa\mathrm{s}\phi \\ \dot{p}\mathrm{s}\kappa\mathrm{s}\phi + p\dot{\kappa}\mathrm{c}\kappa\mathrm{s}\phi + p\dot{\phi}\mathrm{s}\kappa\mathrm{c}\phi \\ \dot{p}\mathrm{c}\kappa - p\dot{\kappa}\mathrm{s}\kappa \end{bmatrix},$$

$$\omega = \begin{bmatrix} \dot{R}_{31}R_{21} + \dot{R}_{32}R_{22} + \dot{R}_{33}R_{23} \\ \dot{R}_{11}R_{31} + \dot{R}_{12}R_{32} + \dot{R}_{13}R_{33} \\ \dot{R}_{21}R_{11} + \dot{R}_{22}R_{12} + \dot{R}_{23}R_{13} \end{bmatrix}.$$

The force Jacobian matrix of the mechanism can be expressed as

$$\boldsymbol{S}_{\mathrm{w}} = \sum_{i=1}^{3} \hat{\boldsymbol{\$}}_{\mathrm{wa},i}^{\mathrm{T}} = \boldsymbol{J}_{xa}\boldsymbol{f} \tag{15}$$

where,

$$\boldsymbol{f} = \begin{bmatrix} f_{wa,1,1} & f_{wa,2,1} & f_{wa,3,1} \end{bmatrix}^{\mathrm{T}}.$$

D. VIRTUAL POWER TRANSMISSIBILITY

The virtual power transmissibility η is defined to evaluate the kinematic performance of the 3-RSR mechanism. The larger η is, the better the kinematic performance is.

$$\eta = \min\left\{\left|\hat{\$}_{\mathrm{wa},1}^{\mathrm{T}}\hat{\$}_{\mathrm{t},1,1}\right|, \left|\hat{\$}_{\mathrm{wa},2}^{\mathrm{T}}\hat{\$}_{\mathrm{t},2,1}\right|, \left|\hat{\$}_{\mathrm{wa},3}^{\mathrm{T}}\hat{\$}_{\mathrm{t},3,1}\right|\right\} \tag{16}$$

Without losing generality, taking $l = 784.8$mm, $a = b = 449.7$mm, $p = 100$mm, $0 \le \theta \le 45°$, the virtual power transmissibility is shown in Fig.5.

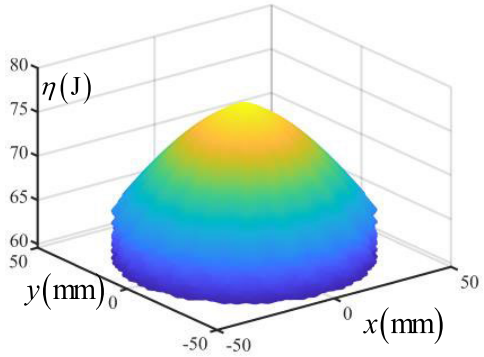

FIGURE 5. Virtual power transmissibility of 3-RSR mechanism.

IV. ESTABLISHMENT OF PERFORMANCE INDICES

The establishment of mechanism performance indices is a process of parameterizing the objective and method of mechanism performance optimization. Based on engineering requirement, the key attributes expected to be obtained are large and high-quality orientational workspace and excellent kinematic performance.

Establishing $\{\theta_{\max}\}_{\max}$ and to evaluate whether the orientational workspace is large enough. Establishing lq to evaluate whether the quality of orientational workspace is high enough. The orientational workspace is required to be large and of high quality. Index $\{\theta_{\max}\}_{\max}$ is defined as the maximum value of $\theta_{\max}$ in global orientational workspace, which is established to evaluate the maximum orientation angle in orientational workspace. The lager $\{\theta_{\max}\}_{\max}$ is, the larger local orientation angle is. Index S is defined as synthesis of $\theta_{\max}$ corresponding to different planes in orientational workspace, which is established to evaluate the global orientation ability (Fig.6-a). The lager the S is, the stronger global orientation ability is. Index lq is defined as $lq = l_1/p$, where l_1 is the value of p corresponding to $\theta_{\max} \ge 45°$, which is established to evaluate proportion of the interval with excellent rotation ability ($\theta_{\max} \ge 45°$) in the global orientational workspace(Fig.6-b). The larger the lq is, the more symmetrical orientational workspace is.

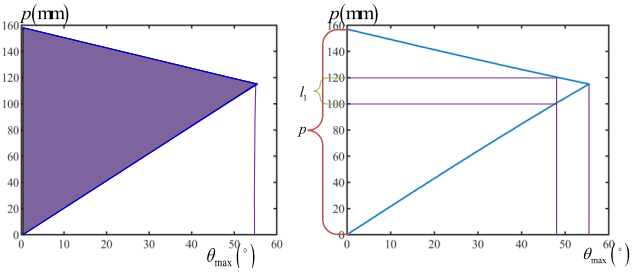

(a) S (b) lq

FIGURE 6. The definition diagrams of S and lq.

Based on (16), η_k is defined as the minimum value of virtual power transmissibility under the determined structure of the mechanism.

$$\eta_{\mathrm{k}} = \min(\eta) \tag{17}$$

The virtual power transmissibility of the mechanism changes with the change of the pose of the mechanism. $\bar{\eta}_W$ (18) is established to respectively evaluate whether the global kinematic performance is excellent. And $\hat{\eta}_W$ (19) is established to respectively evaluate whether the global kinematic performance is steady.

$$\bar{\eta}_W = \frac{\int \eta_k \mathrm{d}x}{V} \tag{18}$$

$$\hat{\eta}_W = \frac{\int \left(\eta_k - \bar{\eta}_w\right)^2 \mathrm{d}x}{V} \tag{19}$$

where V is the orientational workspace volume of the 3-RSR mechanism.

Based on the analysis of orientational workspace, the mechanism has large orientation capability, but in actual use, the mechanism only needs to complete large load work in the area with the best working capability. Therefore, the kinematic performance of the area with the best working capability is investigated as an performance index, that is, the $\bar{\eta}_W$ and $\hat{\eta}_W$ of the orientational workspace in area meeting $\{p \in (100\text{mm}, 120\text{mm}), \theta \in (0, 45°), \varphi \in (0, 360°)\}$, which are selected as the kinematic indices of the mechanism.

V. ANALYTICAL MODEL OF PERFORMANCE INDICES

A. NORMALIZATION OF PARAMETERS

According to the analysis about structure of 3-RSR mechanism, the design variables of the mechanism include two parameters, $\boldsymbol{x} = \{x_1\ x_2\} = \{a\ \lambda_{l/a}\}$. a is the design parameter of moving and static platforms. $\lambda_{l/a} = l/a$, l is the length of the link. The range of initial parameters of the mechanism are set based on topological design, $400 \le a \le 500$mm, $1.5 \le \lambda_{l/a} \le 2$.

In order to meet the requirement of the mechanism for large orientation capability and excellent kinematics performance, the performance indices of $\{\theta_{\max}\}_{\max}$, lq, S, $\bar{\eta}_W$ and $\hat{\eta}_W$ are established. Under the given constraints, the optimization of 3-RSR mechanism can be reduced to a class of constrained nonlinear programming problems, namely

$$\begin{aligned} F(x) = &\max\left(\{\theta_{\max}\}_{\max}\right) \,\&\, \max\left(S\right) \,\&\, \max\left(lq\right) \\ &\&\, \max\left(\bar{\eta}_W\right) \,\&\, \min\left(\hat{\eta}_W\right) \\ \text{s.t.} &\begin{cases} |\mathrm{J}|_{\min} > 0 \\ \theta_S < \theta_{S\max} \\ \theta_R < \theta_{R\max} \\ D < D_0 \end{cases} \end{aligned} \tag{20}$$

B. ESTABLISHMENT OF RSM OF PERFORMANCE INDICES WITHOUT CONSIDERING PARAMETER PERTURBATION

The RSM of indices without considering parameter perturbation is established to lay a foundation for RSM of mean value of indices considering parameter perturbation. The accuracy assessments of the obtained RSM are shown in Table 1. RSM with highest accuracy have been painted in gray in Table 1.

The RSM expressions with the highest accuracy are shown below, which are obtained for the establishment of RSM of performances considering parameter disturbance.

$$\begin{aligned} S = &\ 41100.0956553297a\lambda_{l/a} + 508285.055994179\lambda_{l/a}^2 \\ &+ 282.371284652082a^2 - 3276147.21710864\lambda_{l/a} \\ &- 88532.1629021167a + 4795465.23546571; \\ lq = &\ 0.0119009967815519a\lambda_{l/a} \\ &+ 0.0883885031928216\lambda_{l/a}^2 \\ &+ 0.000154345018279269a^2 \\ &- 0.587491204435973\lambda_{l/a} \\ &- 0.0323832137956043a \\ &+ 1.10829091092029; \\ \{\theta_{\max}\}_{\max} = &\ \text{-}0.0363987373418507\text{a} \\ &+ 17.096621565958\lambda_{l/a}\text{+}26.7211825936555; \\ \hat{\eta}_W = &-724.025855046839\lambda_{l/a}^4 \\ &- 0.000152662927569013a^4 \\ &+ 5204.30374890501\lambda_{l/a}^3 + 0.0296806191847425a^3 \\ &+ 4.69811502392542a\lambda_{l/a} - 13888.882140515\lambda_{l/a}^2 \\ &- 2.09773159066695a^2 + 16062.4363751481\lambda_{l/a} \\ &+ 54.8858932824178a - 7337.17255400874; \end{aligned}$$

TABLE 1. Accuracy of analytical mapping model of performance indices.

	Type	RAAE	RMAE	RMSE	R^2
lq	Linear	0.03954	0.05387	0.05387	0.96491
	Quadratic	0.04783	0.08281	0.05343	0.97499
	Cubic	0.15906	0.31564	0.19218	0.60625
	Quartic	0.14173	0.30245	0.17349	0.77228
$\{\theta_{\max}\}_{\max}$	Linear	0.03525	0.04026	0.04026	0.98282
	Quadratic	0.05997	0.12200	0.07074	0.95501
	Cubic	0.04058	0.10081	0.04834	0.97528
	Quartic	0.04425	0.12438	0.05721	0.97762
S	Linear	0.08302	0.09206	0.09206	0.89449
	Quadratic	0.04697	0.12416	0.06503	0.96394
	Cubic	0.14803	0.35345	0.19395	0.53999
	Quartic	0.0939	0.22704	0.11201	0.85832
$\hat{\eta}_W$	Linear	0.15114	0.16446	0.16446	0.77908
	Quadratic	0.0776	0.20215	0.09823	0.94494
	Cubic	0.11307	0.24798	0.13194	0.87384
	Quartic	0.05447	0.17538	0.07474	0.95474
$\bar{\eta}_W$	Linear	0.10186	0.11227	0.11227	0.87684
	Quadratic	0.02242	0.04763	0.02610	0.99547
	Cubic	0.0245	0.05506	0.02841	0.99283
	Quartic	0.01231	0.04158	0.01668	0.99686

VI. ANALYTICAL MODEL OF OPTIMIZATION OBJECTIVES UNDER PARAMETER PERTURBATION

A. PARAMETER PERTURBATION

Generally, due to the existence of processing error, assembly error, temperature and other factors, there is a perturbation between the actual parameters of the prototype and the theoretical parameters obtained by the optimization design, which makes the performances of the prototype and different from the design performance. To effectively avoid the influence of parameter perturbation, reducing the influence of parameter perturbation should be considered in the optimization design process. In the calculation of each basic parameter, 1000 perturbation points are selected as the actual processing parameter.

The fluctuation degree of mechanism performance caused by parameter perturbation can be calculated as

$$p(h(x)) = \frac{h(x) - \bar{h}(x)}{\bar{h}(x)} \tag{21}$$

where, $h(x)$ represents the performance indices determined above, and $\bar{h}(x)$ represents the average level of corresponding performance indices affected by parameter perturbation.

As shown in Fig. 7, the fluctuation of each performance indices of the mechanism with respect to its mean value under the influence of parameter perturbation is different. For a group of optimization parameters generated by parameter perturbation, the fluctuation coefficient value of the performance indices of the mechanism is expected to be within a

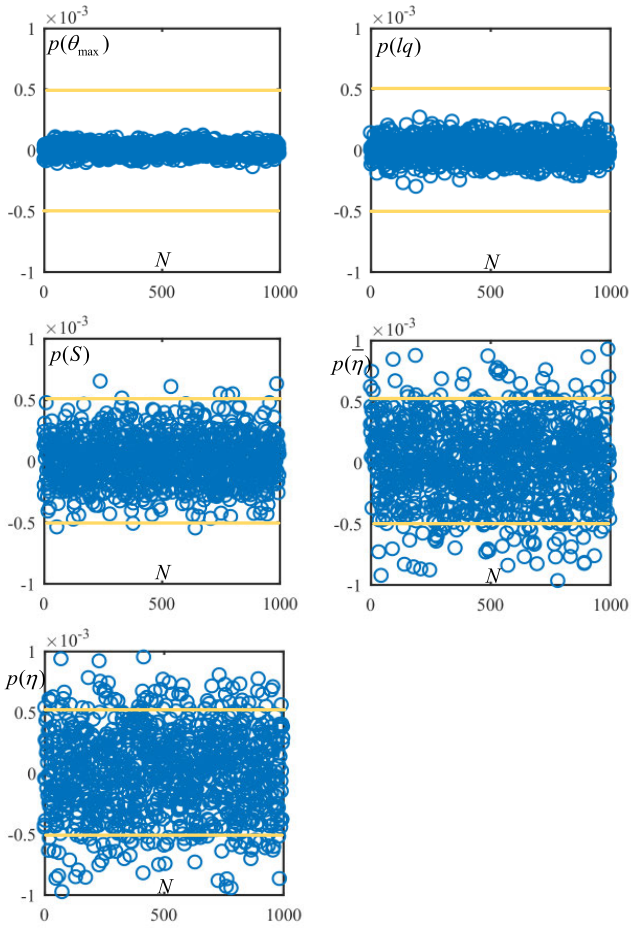

FIGURE 7. Relative dispersion extents of performance indices.

certain range, that is

$$|p(h(x))| \leq \varsigma_{h(x)} \tag{22}$$

where, $\varsigma_{h(x)}$ is the maximum allowable value of the relative fluctuation coefficient of the corresponding performance indices. In this example, the value of $\varsigma_{h(x)}$ is 5×10^{-4}. $N_p(h(x))$ is defined as the number of relative fluctuation coefficients meeting the allowable conditions for corresponding performance indicators in N groups of random values. $\chi_{h(x)}$ is defined as the dispersion coefficients of corresponding performance indices under the influence of parameter perturbation, as shown in (23). The higher value of relative proportion indices the more numbers of performance values are within the acceptable ranges. With more values within acceptable ranges, parallel tracking mechanism is more likely to resist the effect of parameter perturbation and become robust.

$$\chi_{h(x)} = \frac{N_p(h(x))}{N} \tag{23}$$

Therefore, the influence of parameter perturbation can be described by two indices in terms of mean value and relative proportion. The mean value represents its average effect and is used to form objectives in the following content. And the relative proportion shows the overall dispersion level caused by the perturbation. It is utilized to set constraint conditions in this paper as

$$\chi_{h(x)} > \zeta_{h(x)} \tag{24}$$

where, $\zeta_{h(x)}$ is safety factor of performance $h(x)$.

B. ESTABLISHMENT OF RSM OF MEAN VALUE OF PERFORMANCE INDICES

$$F(x) = \max\left(\left\{\bar{\theta}_{\max}\right\}_{\max}\right) \& \max\left(\bar{S}\right) \& \max\left(\overline{lq}\right) \& \max\left(\overline{\bar{\eta}_W}\right) \& \min\left(\overline{\hat{\eta}_W}\right)$$

$$\text{s.t.} \begin{cases} |\mathrm{J}|_{\min} > 0 \\ \theta_S < \theta_{S\max} \\ \theta_R < \theta_{R\max} \\ D < D_0 \\ \chi_{h(x)} > \zeta_{h(x)} \end{cases} \tag{25}$$

The mechanism optimization function considering parameter perturbation is shown in (25).

Based on the RSM of indices without considering parameter perturbation established above, the boundary value of parameter perturbation is considered as the constraint condition, and the RSM of mean value of indices considering parameter perturbation is established. The accuracy assessments of the obtained RSM are shown in Table 2. RSM with highest accuracy have been painted in gray in Table 2.

TABLE 2. Accuracy of analytical mapping model for optimization objectives.

	Type	RAAE	RMAE	RMSE	R^2
$\overline{lq}$	Linear	0.03248	0.07173	0.03779	0.98928
	Quadratic	0.00054	0.00114	0.00064	1.00000
	Cubic	0.00045	0.000918	0.00053	1.00000
	Quartic	0.00068	0.00153	0.00081	1.00000
$\left\{\bar{\theta}_{\max}\right\}_{\max}$	Linear	0.00052	0.00108	0.00062	1.00000
	Quadratic	0.00045	0.00102	0.00054	1.00000
	Cubic	0.00068	0.00150	0.00081	0.99999
	Quartic	0.00063	0.00152	0.00078	0.99999
$\bar{S}$	Linear	0.08570	0.15122	0.09631	0.91158
	Quadratic	0.00134	0.00299	0.00156	0.99998
	Cubic	0.00034	0.00065	0.00041	1.00000
	Quartic	0.00087	0.00163	0.00095	0.99999
$\overline{\hat{\eta}_W}$	Linear	0.09935	0.15768	0.10648	0.91040
	Quadratic	0.01649	0.04203	0.02047	0.99503
	Cubic	0.01132	0.01535	0.01187	0.99886
	Quartic	0.00071	0.00206	0.00096	0.99999
$\overline{\bar{\eta}_W}$	Linear	0.08118	0.11942	0.08759	0.92884
	Quadratic	0.00508	0.01110	0.00583	0.99958
	Cubic	0.00445	0.00588	0.00464	0.99982
	Quartic	0.000842	0.00221	0.00108	0.99999

The RSM expressions with the highest precision are shown, which are the approximate explicit expressions

between the mean value of the performance indices and the parameters of the multi-objective optimization.

$$\begin{aligned}\overline{S} &= -6996.60110684188\lambda_{l/a}^3 \\ &\quad + 0.319133075632282a^3 \\ &\quad + 41080.2177052155a\lambda_{l/a} + 543943.866697879\lambda_{l/a}^2 \\ &\quad + 240.680159694408a^2 - 3335508.94779555\lambda_{l/a} \\ &\quad - 86690.583386284a + 4801791.62546645; \\ \overline{lq} &= -0.00240890656652093\lambda_{l/a}^3 \\ &\quad - 2.01758410796695 * 10^{(-7)}a^3 \\ &\quad + 0.0118990874443818a\lambda_{l/a} \\ &\quad + 0.1004207474583 68\lambda_{l/a}^2 \\ &\quad + 0.000182475376045731a^2 \\ &\quad - 0.607299319902764\lambda_{l/a} - 0.0336829721209771a \\ &\quad + 1.13911708982782; \\ \overline{\{\theta_{\max}\}_{\max}} &= 0.00021696285039816 2a\lambda_{l/a} \\ &\quad - 0.0349936872077747\lambda_{l/a}^2 \\ &\quad + 5.5317315143541 * 10^{-5} * a^2 \\ &\quad + 17.2086721894613\lambda_{l/a} \\ &\quad - 0.0417408577649318a + 26.7442693302875; \\ \overline{\hat{\eta}_W} &= -724.0258550468 39\lambda_{l/a}^4 \\ &\quad - 0.000185225468769718a^4 \\ &\quad + 5229.4807593441\lambda_{l/a}^3 + 0.0356401678491408a^3 \\ &\quad + 4.69461469097792a\lambda_{l/a} - 13956.006592025\lambda_{l/a}^2 \\ &\quad - 2.50613901864399a^2 + 16142.5616717967\lambda_{l/a} \\ &\quad + 67.3126950327253a - 7514.79519447776; \\ \overline{\bar{\eta}_W} &= 560.243396771152\lambda_{l/a}^4 \\ &\quad + 4.07134749553258 * 10^{-5} * a^4 \\ &\quad - 3880.19913600222\lambda_{l/a}^3 - 0.00646454025427559a^3 \\ &\quad - 8.81479875760181a\lambda_{l/a} + 9899.75986065384\lambda_{l/a}^2 \\ &\quad + 0.215734803639072a^2 - 10538.0257167546\lambda_{l/a} \\ &\quad + 23.0302151343259a + 3377.40268282703;\end{aligned}$$

The particle swarm optimization (PSO) based on Isight software is adopted. The analytical mapping models are coded and directly typed in the interface that provided by the Isight software. Then Isight software will execute the optimal calculation.

Pareto frontiers are obtained after the multi-objective optimization, since the five objectives are simultaneously considered. Pareto frontier denotes the nondominant solutions that none of the objective can be improved in value without degrading some of the other objective values. All the solutions on Pareto frontier are deemed to be equally good.

C. POINT PREFERRED STRATEGY

To further ensure the global mean and fluctuation of kinematic performance of the mechanism in the orientational workspace, the global performance index is constructed.

$$G(x) = \max(\sqrt{\overline{\hat{\eta}_W}^2 + \overline{\bar{\eta}_W}^2}), st.\{\hat{\eta}_W < 45 \qquad (26)$$

The final solution can be selected from Pareto frontiers as

$$\text{a} = 34;\ \lambda_{l/a} = 1.830644564;$$

The comparison of orientational workspace and virtual power transfer rate before and after optimization is shown in Fig.8. and Fig.9. Where, the red part represents the comparison of orientational workspace and virtual power transfer rate after optimization. It is obvious that the orientational workspace and virtual power transfer rate after optimization are better than before.

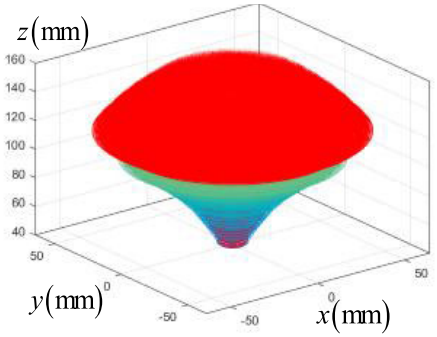

FIGURE 8. Comparison of orientational workspace before and after optimization.

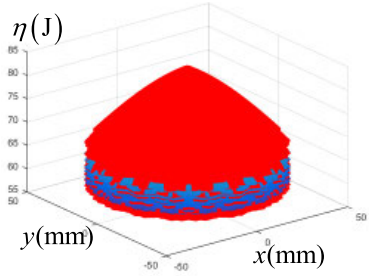

FIGURE 9. Comparison of virtual power transfer rate before and after optimization.

VII. CONCLUSION

Based on the actual requirements of satellite antenna driving mechanism, the multi-objective optimization under the influence of parameter perturbation carried out on 3-RSR mechanism in this paper. Achievements in this process include:

1. To apply 3-RSR mechanisms for the satellite antenna driving mechanism, a multi-objective optimization method based on FIS theory for 3-RSR mechanisms under the influence of parameter perturbation is proposed.

2. The orientational workspace and kinematics performance indices of the mechanism are proposed towards the actual requirements of the satellite antenna driving mechanism and its relationship with the parameters are established. Two RSMs of performance indices without considering and considering parameter perturbation are established to simplify the discrete operation process considering parameter perturbation.

3. The multi-objective optimization of 3-RSR mechanism considering parameter perturbation is completed, and the Pareto frontier is obtained. According to the point preferred strategy, the final value of parameters of the 3-RSR mechanism are determined.

REFERENCES

[1] S. Mauro, A. Battezzato, G. Biondi, and C. Scarzella, "Design and test of a parallel kinematic solar tracker," *Adv. Mech. Eng.*, vol. 7, no. 12, pp. 1–16, Sep. 2015, doi: 10.1177/1687814015618627.

[2] T. Sun, S. Yang, T. Huang, and J. S. Dai, "A way of relating instantaneous and finite screws based on the screw triangle product," *Mechanism Mach. Theory*, vol. 108, pp. 75–82, Feb. 2017.

[3] S. Yang, T. Sun, T. Huang, Q. Li, and D. Gu, "A finite screw approach to type synthesis of three-DOF translational parallel mechanisms," *Mechanism Mach. Theory*, vol. 104, pp. 405–419, Oct. 2016.

[4] C. Chiman and W. Dianjun, "Survey of gimbal drive assembly mechanism of inter-orbit link antenna for tracking and data relay satellites," *Aerosp. Control Appl.*, vol. 36, no. 5, pp. 32–37, Dec. 2010.

[5] J. R. Li, "Elementary analysis on vertex tracking of XY type antenna pedestal," *Mod*, vol. 11, pp. 21–23, Apr. 2010, doi: 10.16652/j.issn.1004-373x.2010.11.026.

[6] B. Lian, T. Sun, Y. Song, Y. Jin, and M. Price, "Stiffness analysis and experiment of a novel 5-DoF parallel kinematic machine considering gravitational effects," *Int. J. Mach. Tools Manuf.*, vol. 95, pp. 82–96, Aug. 2015.

[7] C. Zhang, Y. Wan, D. Zhang, and Q. Ma, "A new mathematical method to study the singularity of 3-RSR multimode mobile parallel mechanism," *Math. Problems Eng.*, vol. 2019, pp. 1–11, Apr. 2019, doi: 10.1155/2019/1327167.

[8] J. Wu, X. L. Chen, and L. P. Wang, "Design and dynamics of a novel solar tracker with parallel mechanism," *IEEE/ASME Trans. Mechatronics*, vol. 21, no. 1, pp. 88–97, Feb. 2016, doi: 10.1109/TMECH.2015.2446994.

[9] H. Yulei, Z. Guoxing, H. Rongwei, and Z. Daxing, "Dynamic modeling of 3-RSR parallel antenna mechanism under wind load based on screw theory," *J. Vibrat. Shock*, vol. 39, no. 19, pp. 174–181, Jul. 2020, doi: 10.13465/j.cnki.Jvs.2020.19.026.

[10] Y. Hou, Y. Zhao, Z. Zhou, D. Zeng, and Y. Yang, "K-inematic and mechanics characteristic analysis of 3-RSR/SP parallel vehicle-borne antenna," *China Mech. Eng.*, vol. 28, no. 23, pp. 2799–2808, Dec. 2017, doi: 10.3969/j.issn.1004-132X.2017.23.005.

[11] R. Di Gregorio, "Inverse position analysis, workspace determination and position synthesis of parallel manipulators with 3-RSR topology," *Robotica*, vol. 21, no. 6, pp. 627–632, Dec. 2003, doi: 10.1017/S0263574703005174.

[12] Y. Qi, T. Sun, and Y. Song, "Multi-objective optimization of parallel tracking mechanism considering parameter uncertainty," *J. Mech. Robot.*, vol. 10, no. 4, Aug. 2018, doi: 10.1115/1.4039771.

[13] C. Gosselin and J. Angeles, "The optimum kinematic design of a planar three-degree-of-freedom parallel manipulator," *J. Mech., Transmiss., Autom. Des.*, vol. 110, no. 1, pp. 35–41, Mar. 1988, doi: 10.1115/1.3258901.

[14] L.-W. Tsai, "Solving the inverse dynamics of a Stewart–Gough manipulator by the principle of virtual work," *J. Mech. Des.*, vol. 122, no. 1, pp. 3–9, Mar. 2000, doi: 10.1115/1.533540.

[15] S. Staicu, "Dynamics of the 6–6 stewart parallel manipulator," *Robot. Comput.-Integr. Manuf.*, vol. 27, no. 1, pp. 212–220, Feb. 2011, doi: 10.1016/j.rcim.2010.07.011.

[16] M. Stock and K. Miller, "Optimal kinematic design of spatial parallel manipulators: Application to linear delta robot," *J. Mech. Des.*, vol. 125, no. 2, pp. 292–301, Jun. 2003, doi: 10.1115/1.1563632.

[17] T. Huang, M. Li, X. M. Zhao, J. P. Mei, D. G. Chetwynd, and S. J. Hu, "Conceptual design and dimensional synthesis for a 3-DOF module of the TriVariant—A novel 5-DOF reconfigurable hybrid robot," *IEEE Trans. Robot.*, vol. 21, no. 3, pp. 449–456, Jun. 2005, doi: 10.1109/TRO.2004.840908.

[18] M. Kong, L. Chen, Z. Du, and L. Sun, "Multi-objective optimization on dynamic performance for a planar parallel mechanism with NSGA-II algorithm," *ROBOT*, vol. 32, no. 2, pp. 271–277, Mar. 2010, doi: 10.3724/SP.J.1218.2010.00271.

[19] T. Sun and B. Lian, "Stiffness and mass optimization of parallel kinematic machine," *Mechanism Mach. Theory*, vol. 120, pp. 73–88, Feb. 2018.

[20] T. Sun, Y. Zhai, Y. Song, and J. Zhang, "Kinematic calibration of a 3-DoF rotational parallel manipulator using laser tracker," *Robot. Comput.-Integr. Manuf.*, vol. 41, pp. 78–91, Oct. 2016.

[21] T. Sun, B. Lian, S. Yang, and Y. Song, "Kinematic calibration of serial and parallel robots based on finite and instantaneous screw theory," *IEEE Trans. Robot.*, vol. 36, no. 3, pp. 816–834, Jun. 2020.

YANG QI was born in Tianjin, China, in 1988. He received the bachelor's degree in mechanical design manufacturing and automation and the M.S. and Ph.D. degrees in mechanical engineering from Tianjin University, in 2011 and 2018, respectively.

From 2018 to 2022, he was a Lecturer with the College of Mechanical Engineering, Tianjin University of Technology and Education. He is the author of 12 patents of innovation and five SCI articles. His research interests include the configuration synthesis of parallel mechanisms with complex motion types, the integrated design of scale parameters and section parameters for multi performance requirements, flight dynamics in microgravity environment, and the prototype construction of parallel mechanisms.

YU WANG was born in Shandong, China. He received the bachelor's degree in mechanical engineering from the Kunming University of Science and Technology, in 2020. He is currently pursuing the master's degree in mechanical engineering with the Tianjin University of Technology and Education. He is the author of two authorized utility model patents and an EI article.

HONG WANG was born in Chongqing, China. He is currently pursuing the bachelor's degree in mechanical engineering with the Tianjin University of Technology and Education. He is the author of a SCI article and two EI articles.